

Simultaneous Electrical Transport and Scanning Tunneling Spectroscopy of Carbon Nanotubes

Brian J. LeRoy,^{*,†} Iddo Heller, Vijay K. Pahilwani, Cees Dekker, and Serge G. Lemay

Kavli Institute of Nanoscience, Delft University of Technology, Lorentzweg 1, 2628 CJ Delft, The Netherlands

Received April 5, 2007; Revised Manuscript Received May 22, 2007

ABSTRACT

We performed scanning tunneling spectroscopy measurements on suspended single-walled carbon nanotubes with independently addressable source and drain electrodes in the Coulomb blockade regime. This three-terminal configuration allows the resistance to the source and drain electrodes to be individually measured, which we exploit to demonstrate that electrons were added to spin-degenerate states of the carbon nanotube. Unexpectedly, the Coulomb peaks also showed a strong spatial dependence. By performing simultaneous scanning tunneling spectroscopy and electrical transport measurements we show that the probed states are extended between the source and drain electrodes. This indicates that the observed spatial dependence reflects a modulation of the contact resistance.

Single-walled carbon nanotubes (SWCNTs) have extremely promising electrical transport properties. In a field-effect transistor geometry, they have been shown to have a higher drive current and transconductance than can be found in Si devices.¹ However, one of the major unresolved issues is the influence of the contacts on their transport properties.^{2–4} The contact material can significantly dope the SWCNT, altering its transport properties. There have been many experimental and theoretical attempts to characterize the effect of different metals on the electrical properties of SWCNT.^{5–7} However, the experiments are limited to measuring the current as a function of source–drain voltage and gate voltage. They do not provide information on, for example, the spatial extent of the doping behavior. Theoretical calculations indicate that the one-dimensional nature of the SWCNT causes the doping effect of the contact to be long-ranged.^{8,9} Measuring the long-range nature of this effect requires an experimental technique which can provide spatial information.

We have designed samples that can be used for electrical transport studies as well as simultaneous scanning tunneling spectroscopy measurements. This allows the high spatial resolution of the scanning tunneling microscope (STM) to be used to study the local density of states in the SWCNT and to provide information about changes in the band structure as a function of position. We have done this by

growing SWCNTs directly on Pt electrodes separated by a trench.¹⁰ A 100 nm trench was etched in a Si wafer with a 250 nm SiO₂ layer to create the separation between the two Pt electrodes which were used as the source and drain electrode. 8 $\mu\text{m} \times 5 \mu\text{m}$ regions were defined by electron-beam lithography at a distance of 1.5 μm from the trench. A Fe:Mo catalyst was deposited in these regions. SWCNTs were grown from the catalyst at 800 °C for 10 min in a flow of ethylene (40 mL/min), methane (910 mL/min), and hydrogen (700 mL/min). The SWCNTs grew randomly from the catalyst region, yielding some SWCNTs which crossed the trench separating the source and drain electrode. Figure 1A is an atomic force microscope image of one such SWCNT crossing the trench between the source and the drain electrode. This growth technique gives many SWCNTs in parallel between the source and drain electrode, but the STM tip selectively probes the properties of only one of these SWCNTs.

Initial studies have shown that probing suspended SWCNTs by scanning tunneling microscopy is a powerful system for understanding quantum transport behavior including Coulomb blockade¹¹ and phonon-assisted tunneling.¹² In this work, we use the STM to perform three-terminal transport measurements as well as study the spatial dependence of transport in the SWCNTs. Figure 1B is a schematic of the measurement setup used for performing simultaneous electrical transport and spectroscopy measurements. The sample voltage was applied between the grounded tip and the source electrode. For the spectroscopy measurements, the differential

* Corresponding author. E-mail: leroy@physics.arizona.edu.

† Current address: Department of Physics, University of Arizona, 1118 E. 4th Street, Tucson, AZ 85721.

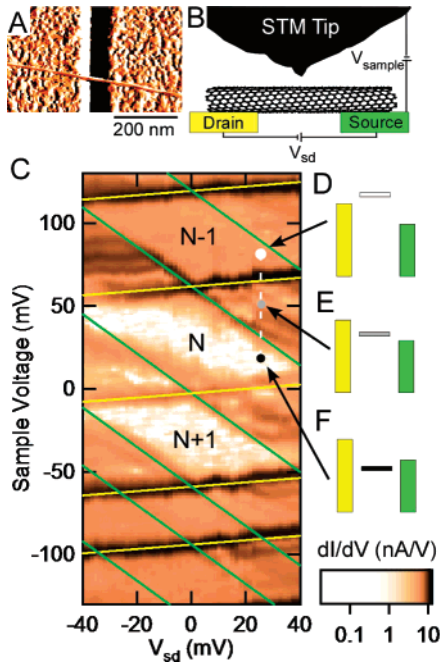


Figure 1. (A) Atomic force microscope image of a SWCNT crossing the trench separating the source and drain electrodes. (B) Schematic diagram showing the setup used to perform simultaneous spectroscopy and resistance measurements on a suspended SWCNT. The sample voltage was applied between the tip and the source electrodes while a constant voltage or current was applied between the source and the drain electrodes. (C) Measured differential conductance as a function of source–drain voltage and sample voltage. The tip current was stabilized at 300 pA at -200 mV before the feedback circuit was switched off and the differential conductance was measured using a lock-in technique. The diamond shaped regions are areas where the number of electrons on the SWCNT is fixed. The colored lines show where a state on the SWCNT aligns with the Fermi level of the source (green) or the drain (yellow) electrode. (D–F) The energy of a state on the SWCNT with respect to the leads for three different sample voltages (corresponding to the white, gray, and black dots). In D, the state is always unoccupied, while in F, it is always occupied and unavailable for tunneling into from the tip. In case E, the probability of occupation is controlled by the relative tunneling rates to the source and drain electrode, which allows these rates to be measured.

conductance $dI_{\text{tip}}/dV_{\text{sample}}$ into the tip was measured. In addition for electrical transport measurements there was a constant current applied between the source and drain electrodes, and the resulting source–drain voltage was recorded. All the measurements were performed in a modified Omicron low-temperature ultrahigh vacuum STM at a temperature of 4.5 K.¹³

Figure 1C plots the differential conductance, $dI_{\text{tip}}/dV_{\text{sample}}$, as a function of the source–drain voltage and the sample voltage for a metallic SWCNT. The image shows diamond shaped regions of low differential conductance outlined by lines of high differential conductance. This is reminiscent of Coulomb blockade measurements in a quantum dot where the differential source–drain conductance as a function of source–drain and gate voltage exhibits diamonds representing regions of fixed numbers of electrons. In this case we have three conducting electrodes: source, drain, and tip. The current goes from the tip into either the source or the drain

electrode. Therefore, we would expect a series of lines when a state on the SWCNT lines up with the Fermi energy of the tip, source, or drain. The strength of each of these lines is proportional to the tunnel rate from the state on the SWCNT to the particular lead. In our case the tunnel rate into the tip is much slower than the tunnel rates into the two leads. As a result, only the two sets of lines that correspond to tunneling into the source and drain are visible (yellow and green lines, Figure 1C), giving a diamond shaped pattern. In Figure 1C, six different occupation numbers are visible, but more than 20 have been observed in other samples.¹¹ Because each line corresponds to the energy needed to align a state on the SWCNT with the Fermi level of one of the leads, the slope of the line gives information about how the energy of the state changes as a function of the sample voltage and the source–drain voltage. Therefore, the slopes give information about the capacitances in the system. The slope of the line corresponding to aligning a state on the SWCNT with the drain electrode is C_s/C_t where C_t and C_s are the capacitances between the SWCNT and the tip and source. The slope for the source electrode is $-(C_d + C_t)/C_t$ where C_d is the capacitance between the SWCNT and the drain. To completely determine the capacitances, we can either use the height of the diamonds, e/C_t , or their width e/C_Σ where C_Σ is the sum of the three capacitances. For the SWCNT show in Figure 1C, we find that $C_t = 4.5$ aF, $C_s = 0.6$ aF, and $C_d = 0.9$ aF. This is in agreement with the previous two-terminal measurements in this type of system where the separate capacitances to the source and drain could not be determined.^{11,12}

At fixed source–drain voltage and varying sample voltage, the tip acts as a gate and controls the number of electrons on the SWCNT. Starting inside the diamond marked with the black circle, the number of electrons is fixed at N . The energy level of the N electron state is shown in Figure 1F where it is below the Fermi level of both the source and the drain electrode. Increasing the sample voltage allows the N electron state to rise above the Fermi level of the source electrode (Figure 1E). Therefore, there is current flowing through the N electron state due to the source–drain voltage. This leads to the N electron state being partially occupied, the degree of occupation being dependent on the relative tunneling rates to the source and drain electrode. When the state is empty, it is possible for an electron from the tip to tunnel into it giving rise to a new conduction channel from the tip to the source. Assuming that the state is not degenerate, this causes a change in the tip current proportional to the probability of the state being empty, $\gamma_d/(\gamma_s + \gamma_d)$ where γ_s and γ_d are the tunnel rates to the source and drain electrodes. As the voltage is increased further (Figure 1D), the N electron state rises above both the source and the drain electrode. In this case the state is always available for tunneling into from the tip, and the probability of the state being empty is 1. Therefore the current has another step proportional to $\gamma_s/(\gamma_s + \gamma_d)$. The ratio between these two steps gives the ratio between the coupling to the source and drain electrode. Figure 2A shows the expected

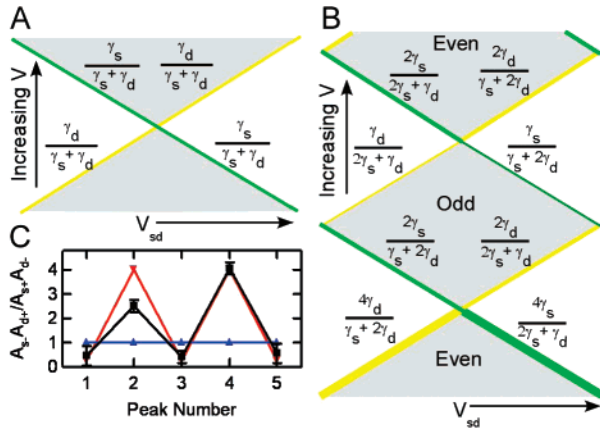


Figure 2. Diagrams showing the expected strength of the Coulomb blockade peaks as a function of source–drain voltage and number of electrons for (A) a nondegenerate state on the SWCNT and (B) a spin-degenerate state. (C) Graph plotting the relative amplitude of the source and drain peaks for the SWCNT shown in Figure 1C. The black squares are the experimentally measured data, the red triangles are the calculated result for a spin-degenerate state, and the blue triangles are the calculated result for a nondegenerate state on the SWCNT.

strength of the source and drain peaks for the case of a nondegenerate state on the SWCNT.

The situation is more complicated if the state on the SWCNT is spin-degenerate: there is then a difference in the tunneling rates depending on the occupation of the state.^{14,15} If the SWCNT has an even number of electrons, there are two ways to tunnel onto it, either spin up or spin down, while if there are an odd number of electrons on it there is only one way to tunnel. This leads to a difference in the tunneling rates for even and odd numbers of electrons and depending on the direction of the source–drain voltage. Figure 2B shows the strength of the expected lines for the case of a spin degenerate level on the SWCNT. To see the effect of the level degeneracy, we measure the amplitude of the source and drain peaks for both positive and negative source–drain voltage. In the case of spin degenerate levels, the quantity $A_{s-}A_{d+}/A_{s+}A_{d-} = 4$ for an even number of electrons on the SWCNT and $1/4$ for an odd number where $A_{s(d)+(-)}$ is the amplitude of the source (drain) peak for positive (negative) source–drain voltage (see Supporting Information). If the state on the SWCNT is nondegenerate, then this ratio is 1 for any number of electrons. We have measured the ratio of these peaks for the SWCNT shown in Figure 1C, and the results are plotted in Figure 2C. There is a clear alternating pattern in the ratio where the odd numbered peaks range from 0.4 to 0.5, while the even numbered ones range from 2.5 to 4.1. This alternating behavior indicates that the states on the SWCNT are spin-degenerate and electrons are added with alternating spin.

The STM furthermore allows the positional dependence of the tunneling rates to be studied. Figure 3 shows the effect on the electronic spectra of moving the tip to different locations along the nanotube between the source and the drain electrode. Figure 3A is a topographic image of the SWCNT crossing the trench with the source electrode on the left and the drain electrode on the right. The three locations where

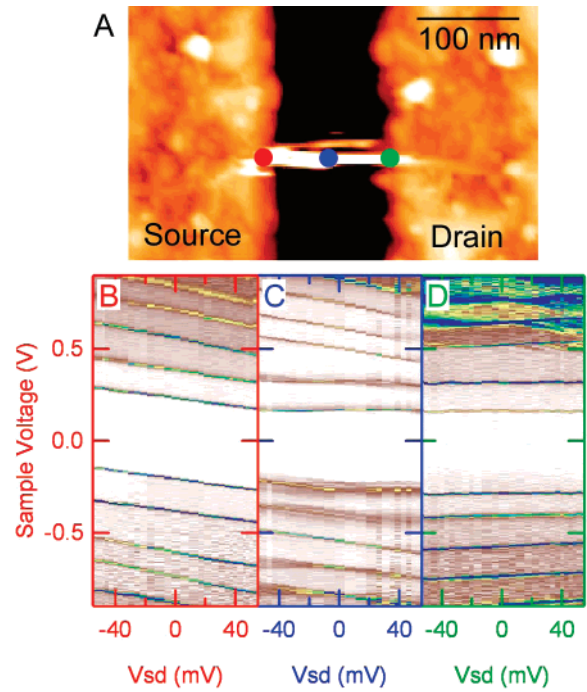


Figure 3. (A) STM topographic image showing the suspended SWCNT going between the source (left) and the drain (right) electrodes. The colored circles indicate the locations where the differential conductance measurements in (B) red, (C) blue, and (D) green were acquired. (B–D) Differential conductance as a function of source–drain voltage and source voltage at three different positions along the suspended SWCNT. As the tip is moved, qualitatively different differential conductance measurements are obtained. The white areas are low differential conductance while the blue lines represent high differential conductance. Electrons from the tip couple more strongly to the lead closest to the tip as indicated by the changing strength of the lines in the differential conductance images.

the differential conductance measurements were taken are indicated by the colored circles: the red circle is shown in Figure 3B, the blue circle is shown in Figure 3C, and the green circle is shown in Figure 3D. All of the spectroscopy data were obtained under the same experimental conditions; the setpoint current was stabilized at 500 pA with $V_{\text{sample}} = -1.0$ V. The differential conductance graph at each of these locations (shown in Figure 3B–D) is qualitatively different. As the tip is moved from the left to the right, the downward sloped lines disappear and upward sloping lines appear. Because the downward sloped lines are due to states coupled to the source electrode and the upward sloping lines arise from states coupled to the drain electrode, their changing strength indicates that the coupling to the source and drain electrode is strongly dependent on the position of the tip. Figure 3C is taken near the center of the nanotube and indicates that electrons tunneling from the tip couple to both the source and the drain side, albeit better to the drain in this case. Near the edges, however, the electrons only couple to the nearer electrode, as shown in Figure 3B,D. This produces stronger lines in one direction unlike Figure 1C where complete diamonds are visible due to nearly symmetric coupling. Moving along the nanotube, the ratio of the peaks for the source to the drain side goes from much more than 10 in

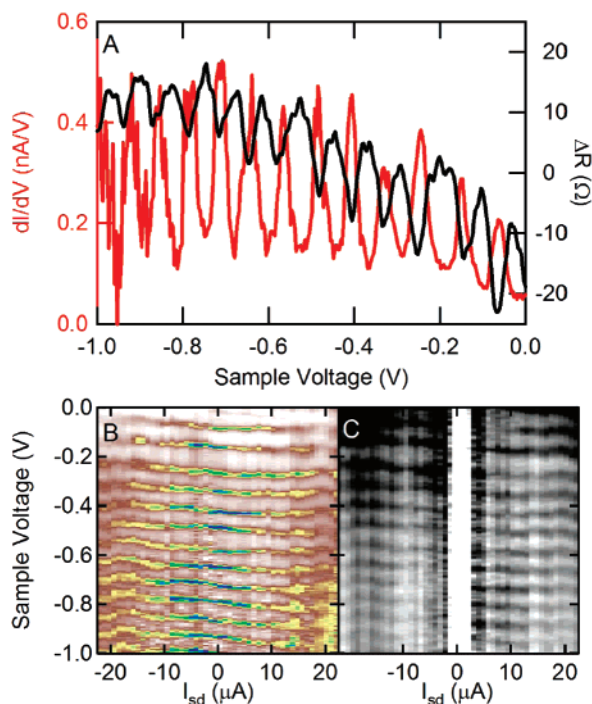


Figure 4. (A) Simultaneous measurement of the differential conductance, dI/dV , and change in resistance as a function of source voltage. For every peak in the differential conductance there is a corresponding dip in the resistance indicating that a new state moves into the source–drain bias window. (B and C) Images show the (B) differential conductance and (C) change in resistance as a function of source–drain current and sample voltage. All of the lines in the differential conductance measurement (yellow and blue areas) also appear in the resistance measurement indicating that all of the states being probed are extended between the source and drain electrode.

Figure 3B to less than 0.1 in Figure 3D. We have observed this general trend of stronger coupling to the nearer electrode in all five SWCNTs that we have measured using our three-terminal technique (see Supporting Information for data from a second SWCNT). This is very different than what is expected from a simple picture of a Coulomb blocked quantum dot where the coupling to the source and drain electrodes is determined by the local overlap of the wave function on the nanotube with those of the electrodes. Because the tip is probing the same state at each position, the coupling to the electrodes should not be position dependent.

One possible explanation for the strong position dependence is that the tip is probing states in the SWCNT that are localized near only one of the source and drain electrodes. Such localized states might result for example from band bending near the contacts. To test for the possible presence of such localized states, we performed simultaneous electrical transport measurements and spectroscopy measurements. We measured both the current from the tip and the voltage drop between the source–drain contacts while a constant current was applied between the source and the drain electrodes. Figure 4A shows the simultaneous spectroscopy and resistance measurements. The spectroscopy data (shown in red) exhibit a series of sharp peaks. Each peak indicates that a state of the SWCNT is crossing the Fermi level of the drain

electrode and entering the source–drain bias window. This state leads to a new conduction path between the source and the drain electrodes, as reflected by the corresponding dip in the resistance of the SWCNT (shown in black). Figure 4B,C are simultaneous measurements of the differential conductance and change in resistance of the SWCNT as a function of both source–drain current and sample voltage. All of the lines in the differential conductance image (Figure 4B) are represented in the resistance image (Figure 4C) indicating that all of the states in the SWCNT couple to both the source and the drain electrode and contribute to the source–drain current. This signifies that the states being probed by the spectroscopy measurement are extended over the whole region between source and drain. Therefore, their positional dependence must arise from another source. One possible origin is the Schottky barriers that are known to form at the interface between semiconducting SWCNTs and metal electrodes.³ The presence of the charged STM tip could influence this barrier leading to the observed spatially dependent coupling between the SWCNT and the electrodes. However, we also see a similar effect on metallic SWCNTs where the Schottky barriers are presumably absent. Therefore, more experimental and theoretical work is needed to understand the exact mechanism leading to the strong modulation of the contact resistance.

In summary, we have developed a technique for performing simultaneous electrical transport and spectroscopy measurements on carbon nanotubes. This allowed us to obtain local density of states information as a function of transport properties such as source–drain current or gate voltage. We have demonstrated how this technique is able to probe the resistance between the SWCNT and the source and drain electrodes. This is a measurement that is not possible without the addition of the third tunneling lead, the STM tip. Conventional three-terminal measurements with a gate electrode only give the product of the tunnel rate to the source and drain electrode but not the individual rates. By examining the strength of the spectroscopy peaks, we found evidence of electrons being added to spin degenerate states on the SWCNT. Interestingly, we observed that the coupling to the source and drain electrodes was strongly dependent on the position of the tip. This indicates that the contacts play a crucial role in determining the transport properties of the SWCNT.

Acknowledgment. This research was funded by Stichting voor Fundamenteel Onderzoek der Materie (FOM), The Netherlands Organization for Scientific Research (NWO), and by NanoNed.

Supporting Information Available: Calculation of tip tunnel current for nondegenerate and spin-degenerate cases. Supplemental figure showing spatial dependence of spectroscopy. This material is available free of charge via the Internet at <http://pubs.acs.org>.

References

- (1) Avouris, P.; Appenzeller, J.; Martel, R.; Wind, S. J. *Proc. IEEE* **2003**, *91*, 1772.
- (2) Derycke, V.; Martel, R.; Appenzeller, J.; Avouris, P. *Appl. Phys. Lett.* **2002**, *80*, 2773.

- (3) Heinze, S.; Tersoff, J.; Martel, R.; Derycke, V.; Appenzeller, J.; Avouris, Ph. *Phys. Rev. Lett.* **2002**, *89*, 106801.
- (4) Javey, A.; Guo, J.; Wang, Q.; Lundstrom, M.; Dai, H. J. *Nature* **2003**, *424*, 654.
- (5) Mann, D.; Javey, A.; Kong, J.; Wang, Q.; Dai, H. J. *Nano Lett.* **2003**, *3*, 1541.
- (6) Shan, B.; Cho, K. J. *Phys. Rev. B* **2004**, *70*, 233405.
- (7) Kim, W.; Javey, A.; Tu, R.; Cao, J.; Wang, Q.; Dai, H. J. *Appl. Phys. Lett.* **2005**, *87*, 173101.
- (8) Leonard, F.; Tersoff, J. *Phys. Rev. Lett.* **1999**, *83*, 5174.
- (9) Xue, Y. Q.; Ratner, M. A. *Appl. Phys. Lett.* **2003**, *83*, 2429.
- (10) Kong, J.; LeRoy B. J.; Lemay, S. G.; Dekker, C. *Appl. Phys. Lett.* **2005**, *86*, 112106.
- (11) LeRoy, B. J.; Lemay, S. G.; Kong, J.; Dekker, C. *Appl. Phys. Lett.* **2004**, *84*, 4280.
- (12) LeRoy, B. J.; Lemay, S. G.; Kong, J.; Dekker, C. *Nature* **2004**, *432*, 371.
- (13) LeRoy, B. J.; Kong, J.; Pahilwani, V. K.; Dekker, C.; Lemay, S. G. *Phys. Rev. B* **2005**, *72*, 075413.
- (14) Cobden, D. H.; Bockrath, M.; McEuen, P. L.; Rinzler, A. G.; Smalley, R. E. *Phys. Rev. Lett.* **1998**, *81*, 681.
- (15) Bonet, E.; Deshmukh, M. M.; Ralph, D. C. *Phys. Rev. B* **2002**, *65*, 045317.

NL0708112